Nonreciprocal Optical Dissipation Based on Direction-Dependent Rabi Splitting

Yu Shi, Qian Lin, Momchil Minkov, and Shanhui Fan, *Fellow, IEEE*

(Invited Paper)

***Abstract*—We consider a ring resonator with two resonant modes undergoing dynamic modulation. Using the Floquet analysis, we show that with a proper choice of modulation profile, such a resonator can achieve a direction-dependent Rabi splitting of its Floquet eigenstates, which results in direction-dependent dissipation and nonreciprocal transmission for waves. We numerically demonstrate this nonreciprocal effect and show that a realistic refractive index modulation of the ring can result in significant transmission in one direction and near complete dissipation in.**

***Index Terms*—Nonreciprocal wave propagation, optical isolators, optical modulation.**

I. Introduction

NONRECIPROCAL optical devices such as optical isolators and circulators are fundamental building blocks in many important optical technologies used in optical communications, laser feedback protection, and optical computing [1]–[3]. Traditionally, reciprocity is broken with the use of magneto-optical materials under a static magnetic field. While this approach is attractive in that it is passive, most optoelectronic materials do not exhibit intrinsic magneto-optical responses, and therefore it is difficult to achieve magneto-optical effects in micro and nanophotonic devices on a CMOS compatible platform [4]–[9]. As a way to circumvent this difficulty, it has been recently proposed and demonstrated that complete optical isolation can be achieved by a spatiotemporal modulation of refractive index [10]–[21]. These recent developments are related to earlier observations of non-reciprocity in dynamically modulated systems [22], [23]. Although this method is active and requires external energy input to drive the index modulation, it is compatible with most optoelectronic materials, most notably silicon. As such, in recent years, increasing efforts have been dedicated to designing nonreciprocal optical components using active nanophotonic devices.

In most of the existing works on dynamic optical isolators, the refractive index modulation results either in the effects of a nonreciprocal phase shift or a nonreciprocal modal conversion. To achieve optical isolation based on either effects requires additional structures such as interferometers or filters [10], [11], [15]–[17]. On the other hand, an ideal integrated isolator should directly provide a nonreciprocal intensity response. It is therefore desirable to design dynamic isolators that directly generate nonreciprocal intensity response without the need of additional filters.

In this work, we present a dissipative nonreciprocal device based on refractive index modulation. The device consists of a micro-ring resonator that supports two lossy modes, and the dynamic modulation is applied at a frequency that is equal to the difference between the photonic modes' frequencies. Using the Floquet analysis, we show that such dynamic modulation can result in a direction-dependent Rabi splitting effect between the photonic modes, such that an incident light can be critically coupled to the lossy photonic modes in only one propagation direction. With coupled mode theory, we demonstrate that such direction-dependent Rabi splitting can lead to significant transmission in the forward direction, and near complete dissipation in the backward direction. Finally, we provide a set of first-principle simulation results on the micro-ring resonator and observe excellent agreement with the Floquet analysis and coupled mode theory. Thus, we show that by deliberately incorporating loss into dynamically modulated systems, we can obtain nonreciprocal optical dissipation in a compact device. Related to our work, recently, nonreciprocal optical dissipation has also been demonstrated on the opto-mechanical platform through the Brillouin scattering induced transparency (BSIT) [20]. Our work differs here in that we focus on the effects of refractive index modulation.

The paper is organized as follows. In Section II, we present the photonic structure and provide a detailed theoretical analysis using the Floquet analysis and coupled mode theory. The analysis reveals the effects of modulation-induced Rabi splitting between the Floquet modes, which can be used to achieve direction-dependent dissipation. In Section III, we numerically demonstrate such directional dissipation with a modulated ring resonator, where the modulation induces nonreciprocal Rabi splitting between its whispering gallery modes. Finally,

Manuscript received January 18, 2018; revised March 3, 2018; accepted March 6, 2018. Date of publication March 9, 2018; date of current version June 20, 2018. This work was supported in part by the Defense Advance Research Project Agency under Grant HR00111720034, and in part by the Air Force Office of Scientific Research under Grant FA9550-17-1-0002, and in part by the Swiss National Science Foundation under Project P2ELP2_165174. *(Corresponding authors: Yu Shi and Shanhui Fan.)*

Y. Shi, M. Minkov, and S. Fan are with the Department of Electrical Engineering, Ginzton Laboratory, Stanford University, Stanford, CA 94305 USA (e-mail: shiy@stanford.edu; mminkov@stanford.edu; shanhui@stanford.edu).

Q. Lin is with the Department of Applied Physics, Ginzton Laboratory, Stanford University, Stanford, CA 94305 USA (e-mail: linqian@stanford.edu).

Color versions of one or more of the figures in this paper are available online at http://ieeexplore.ieee.org.

Digital Object Identifier 10.1109/JSTQE.2018.2814792

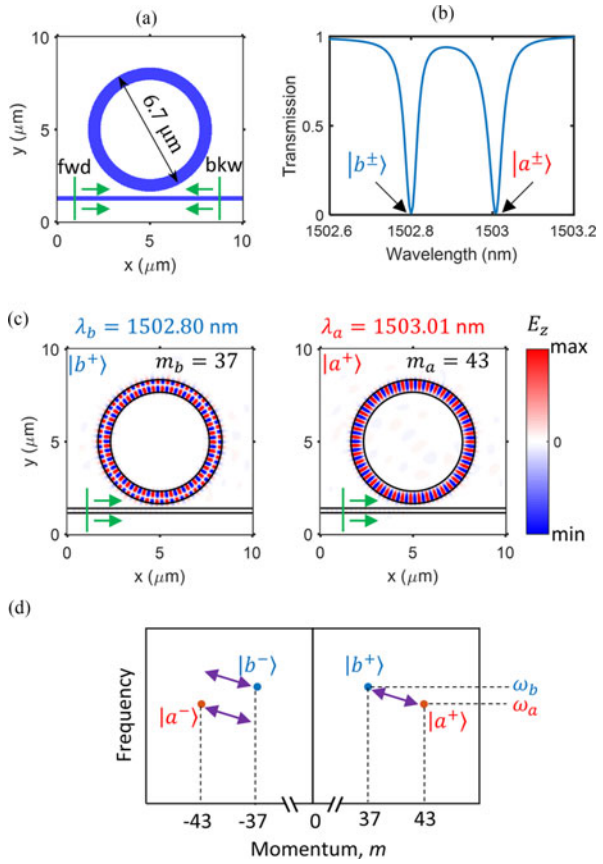

Fig. 1. (a) Schematic of the ring resonator coupled to the external waveguide. The forward direction is defined to be from left to right, and the backward direction is defined to be from right to left. (b) Transmission spectrum through the ring resonator in the absence of modulation. (c) Field profiles showing the two modes of the ring. Mode $|b^+\rangle$ is a quasi-odd guided mode with momentum $m_b = 37$, and mode $|a^+\rangle$ is a quasi-even guided mode with momentum $m_a = 43$. (d) Dispersion diagram of modes $|a^{\pm}\rangle$ and $|b^{\pm}\rangle$. With the appropriate index modulation shown as the purple arrow, one can achieve phase-matched photonic transition between forward modes, but the photonic transition is phase-mismatched for backward modes.

in Section IV, we summarize our work and provide an outlook on such nonreciprocal devices.

II. Theoretical Analysis

A. Two-state Photonic System

To demonstrate the effect of direction-dependent Rabi-splitting and dissipation, we consider the structure shown in Fig. 1(a), which consists of a ring resonator structure coupled to an external straight waveguide. Such ring resonator has intrinsic loss through either radiation or absorption, and it supports both clockwise (CW) and counter-clockwise (CCW) modes. As we will show in the later section, the breaking of reciprocity arises through a photonic transition between some of these resonance modes as induced by dynamic modulation. For the purpose of inducing the transition, the frequency difference between some of the modes needs to be comparable to the modulation frequencies [24]. Thus, the geometry of the ring is designed to support modes with frequencies that are relatively close to each other. For the structure in Fig. 1(a), both the external waveguide and the ring waveguide are made of silicon and have a relative permittivity of 12. The slab waveguide has a width of 250 nm, and it is single-moded in the near infrared optical frequency. The ring waveguide has an outer diameter of 6.7 μm and a width of 675 nm. The straight waveguide and the ring are separated by a gap of 250 nm so that an input mode from the waveguide is critically coupled with at least one mode of the ring. The forward direction is defined as sending the light into the ring from left to right (coupling to its CCW rotating waves), and the backward direction is defined to be from right to left (coupling to its CW rotating waves).

We use the finite-difference frequency-domain (FDFD) method [25], [26] to characterize the passive device in Fig. 1(a) in the absence of dynamic modulation. The spatial resolution of the finite-difference grid is chosen to be $\Delta x = \Delta y = 25$ nm, and the boundaries of the simulation domain are surrounded by 15 layers of stretched-coordinate perfectly-matched layers (SC-PMLs) [25], [27] to suppress spurious reflections at the edges of the simulation. The geometry of the ring is designed to support two modes with different momenta but are close in frequency. As an illustration, we consider first the forward propagation scenario where we excite the system using a source at the left end of the straight waveguide. The transmission spectrum is obtained by analyzing the field at the right end of the waveguide and is plotted in Fig. 1(b), which shows two adjacent modes that are critically coupled to the straight waveguide: mode $|a^+\rangle$ at wavelength $\lambda_a = 1503.01$ nm ($\omega_a = 2\pi \times 199.4635$ THz), and mode $|b^+\rangle$ at wavelength $\lambda_b = 1502.80$ nm ($\omega_b = 2\pi \times 199.4914$ THz). Here, the "+" notation denotes the mode that is rotating in the CCW direction, and is coupled to a forward-propagating wave. By inversion symmetry, such a ring also supports CW rotating modes $|a^-\rangle$ and $|b^-\rangle$ that are critically coupled to the backward-propagating wave at wavelengths λ_a and λ_b respectively, where the "$-$" denotes a clockwise rotating wave that is coupled to a backward-propagating input wave. These optical modes are intrinsically lossy due to the bending loss of the ring waveguide. From the transmission curve in Fig. 1(b), we find that the linewidths of modes $|a^+\rangle$ and $|b^+\rangle$ are $2\gamma_a = 6.4$ GHz and $2\gamma_b = 4.8$ GHz, respectively. The linewidths have contributions from both radiation loss and coupling loss to the straight waveguide. These two contributions are designed to be approximately equal in order to satisfy the critical coupling condition.

In Fig. 1(c), we show the field profiles of the modes $|a^+\rangle$ and $|b^+\rangle$. Mode $|a^+\rangle$ is a quasi-even mode with respect to the center of the ring waveguide, and it has an azimuthal order of $m_a = 43$, which defines its momentum. Mode $|b^+\rangle$ is a quasi-odd mode with respect to the center of the ring waveguide, and it has a momentum of $m_b = 37$. By symmetry, the backward propagating modes $|a^-\rangle$ and $|b^-\rangle$ have very similar field profiles as $|a^+\rangle$ and $|b^+\rangle$, with momenta $-m_a = -43$ and $-m_b = -37$, respectively.

Having discussed the properties of the passive ring resonator, we now discuss how dynamic modulation can break the reciprocity between the forward (CCW rotating) and backward (CW rotating) modes. With their frequency and momentum information, modes $|a^{\pm}\rangle$ and $|b^{\pm}\rangle$ can be represented on a dispersion diagram shown in Fig. 1(d). By the mechanism of photonic transition [10], [28], we can induce coupling between

modes $|a^+\rangle$ and $|b^+\rangle$ by harmonically modulating the permittivity $\varepsilon(\mathbf{r},\ t)$ as

$$\varepsilon\left(\mathbf{r},\ t\right)=\varepsilon_s\left(\mathbf{r}\right)+\delta\left(\mathbf{r}\right)\cos\left(\Omega t+\varphi\left(\mathbf{r}\right)\right), \tag{1}$$

where $\varepsilon_s(\mathbf{r})$ is the time independent relative permittivity as shown in Fig. 1(a), $\Omega=\omega_b-\omega_a=2\pi\times 27.7$ GHz is the modulation frequency, and $\delta(\mathbf{r})$ and $\varphi(\mathbf{r})$ are the modulation amplitude and phase profile, respectively. In particular, the phase of the modulation, $\varphi(\mathbf{r})$, carries a momentum of $M=m_b-m_a=-6$, which induces a phase-matched coupling between forward modes $|a^+\rangle$ and $|b^+\rangle$. The same modulation, however, is phase-mismatched for the coupling between backward modes $|a^-\rangle$ and $|b^-\rangle$. Such a difference in coupling between forward and backward modes breaks reciprocity and gives rise to the direction-dependent Rabi splitting phenomena described in the next section below.

B. Modulation-induced Direction-dependent Rabi Splitting

To theoretically treat the dynamics of the modulated ring system, we first start by briefly reviewing concepts from the Floquet theorem in the context of a modulated optical system. In the absence of modulation, the modes of the ring resonator in Fig. 1(a) can be described by a Hamiltonian H_0, which supports two sets of degenerate eigenstates $|a^\pm\rangle$ and $|b^\pm\rangle$ at frequencies ω_a and ω_b, respectively. The spectrum of H_0 is represented in the left panel of Fig. 2(a), and by definition, the states satisfy

$$H_0\left|a^\pm\right\rangle=\omega_a\left|a^\pm\right\rangle,\quad H_0\left|b^\pm\right\rangle=\omega_b\left|b^\pm\right\rangle. \tag{2}$$

Now, we introduce a spatiotemporal modulation to this two-level system, such that the total Hamiltonian, $H(t)$, becomes

$$H\left(t\right)=H_0+V\cos\left(\Omega t+\phi\right), \tag{3}$$

where V and ϕ represent the amplitude and phase of the modulation profile, which are related to $\delta(\mathbf{r})$ and $\varphi(\mathbf{r})$ in (1), respectively.

Because $H(t)$ in (3) is time-periodic with period $T=2\pi/\Omega$, the interaction between modes $|a^\pm\rangle$ and $|b^\pm\rangle$ can be understood with the Floquet theorem [29], which states that the solution to the time-dependent Hamiltonian, denoted as $|\psi(t)\rangle$, can be written as

$$|\psi\left(t\right)\rangle=e^{i\epsilon t}\left|u(t)\right\rangle, \tag{4}$$

where ϵ is the Floquet quasi-energy, and $|u(t)\rangle=|u(t+T)\rangle$ is the Floquet eigenstate of the Hamiltonian $[H(t)+i\partial_t]$ with eigenvalue ϵ [29]:

$$\left[H\left(t\right)+i\partial_t\right]|u(t)\rangle=\epsilon\,|u(t)\rangle. \tag{5}$$

Because $|u(t)\rangle$ is periodic, it suffices to consider the quasi-energy ϵ in the first Floquet Brillouin zone bounded by $\omega_b-\Omega/2$ and $\omega_b+\Omega/2$, as shown on the right panel of Fig. 2(a).

In the absence of modulation, i.e., when $V=0$, the Floquet eigenstates of (3) are $e^{i\omega_a t}|a^\pm\rangle$ and $e^{i\omega_b t}|b^\pm\rangle$. Thus, aside from a phase factor, the Floquet eigenstates are the same as the eigenstates of H_0. Since frequencies ω_a and ω_b are separated by exactly the modulation frequency Ω, the Floquet eigenstates

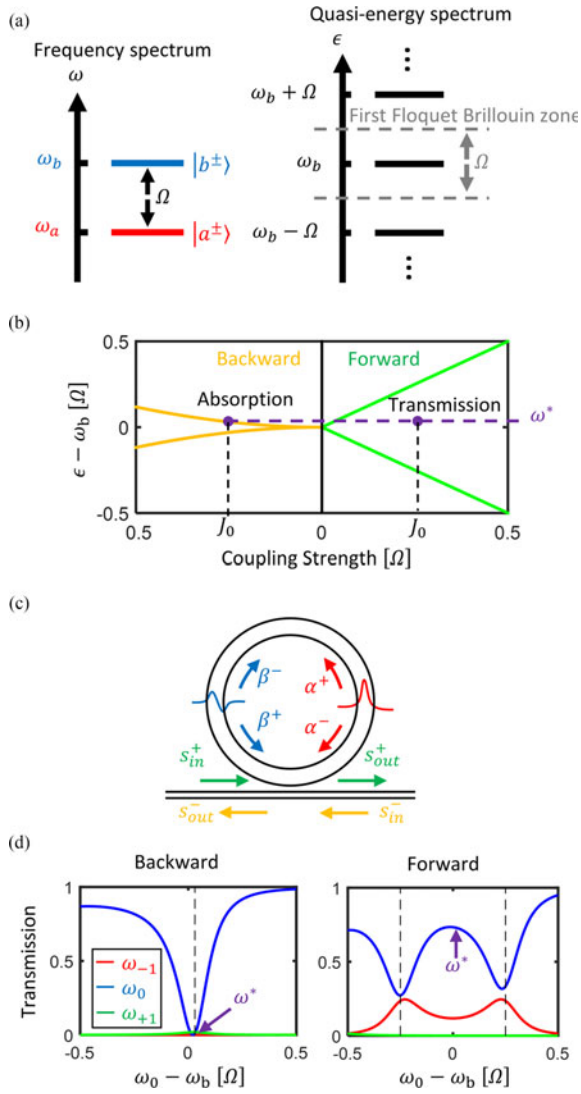

Fig. 2. (a) (Left) Frequency spectrum of the unmodulated ring, showing a pair of eigenmodes with frequencies separated by Ω, and (right) quasi-energy spectrum of the same ring undergoing a modulation at the frequency Ω but with the strength of the modulation set to zero. The first Floquet Brillouin zone, as marked by the gray dotted lines, has a width that is equal to the modulation frequency Ω. In the Floquet picture, modes at ω_a and ω_b are degenerate at every $\epsilon=\omega_b+n\Omega$, where n is an integer. (b) Through a spatiotemporal modulation, the Floquet quasi-energies experience different amounts of Rabi splitting in the forward and backward directions. Such direction-dependent splitting can be used for nonreciprocal optical absorption. (c) Schematic representation of the parameters in coupled mode theory, where the input and output amplitudes and the modal amplitudes are explicitly labeled. (d) Coupled mode theory calculation of the transmitted wave amplitude at frequencies $\omega_n\equiv\omega_0+n\Omega$ in both the forward and backward directions, as a function of the input wave frequency ω_0. The black dotted lines indicate the locations of the Floquet quasi-energies, which predict the locations of the transmission/absorption resonances.

$|a^\pm\rangle$ and $|b^\pm\rangle$ are degenerate without modulation, i.e., they have the same quasi-energy $\epsilon=\omega_b$.

In the presence of modulation, i.e., when $V\neq 0$, with the above choice of modulation frequency Ω and modulation profile $\delta(\mathbf{r})$ and $\varphi(\mathbf{r})$ as discussed in (1), the degeneracy in the Floquet eigenstates would be lifted in different ways depending on the direction of the modes. The lifting of degeneracy due to dynamic modulation is commonly referred to as Rabi splitting [30]. Thus, here we propose to achieve a direction-dependent

Rabi splitting. Recall that the modulation phase profile, $\varphi(\mathbf{r})$, is chosen to carry a momentum $M = m_b - m_a$ as shown in Fig. 1(d). Such a choice of modulation results in phase-matched hence strong coupling between modes $|a^+\rangle$ and $|b^+\rangle$, as well as phase-mismatched hence weak coupling between modes $|a^-\rangle$ and $|b^-\rangle$. We denote

$$J \equiv \left\langle a^+ \right| V e^{-i\phi} \left| b^+ \right\rangle \tag{6}$$

as the strength of the modulation-induced coupling between modes $|a^+\rangle$ and $|b^+\rangle$, which can be calculated by integrating the modal overlap over the modulation profile.

Because the Hamiltonian in (3) is time-periodic with periodicity $2\pi/\Omega$, we can study the dynamics of the Floquet eigenstates by expanding $|u(t)\rangle$ into Fourier components:

$$|u(t)\rangle = \sum_{n=-\infty}^{\infty} e^{in\Omega t} \left(p_n^{\pm} \left| a^{\pm} \right\rangle + q_n^{\pm} \left| b^{\pm} \right\rangle \right), \tag{7}$$

where $p_n^{\pm}$ and $\beta_n^{\pm}$ describe the amplitude of the n-th Fourier amplitude when $|u(t)\rangle$ is projected onto modes $|a^{\pm}\rangle$ and $|b^{\pm}\rangle$, respectively. We substitute (7) into the eigenvalue equation in (5) and perform an inner product with $\langle a^{\pm}|$ and $\langle b^{\pm}|$, which gives a series of independent 2 by 2 blocks at a given Fourier component n. In the forward direction, we have

$$\begin{pmatrix} \omega_b - n\Omega & J \\ J^* & \omega_b - n\Omega \end{pmatrix} \begin{pmatrix} p_{n-1}^+ \\ q_n^+ \end{pmatrix} = \epsilon \begin{pmatrix} p_{n-1}^+ \\ q_n^+ \end{pmatrix}, \tag{8}$$

and in the backward direction, we have

$$\begin{pmatrix} \omega_b - (n+2)\,\Omega & J^* \\ J & \omega_b - n\Omega \end{pmatrix} \begin{pmatrix} p_{n+1}^- \\ q_n^- \end{pmatrix} = \epsilon \begin{pmatrix} p_{n+1}^- \\ q_n^- \end{pmatrix}. \tag{9}$$

From the equations above, the eigenvalues in the first Floquet Brillouin zone are, in the forward direction,

$$\epsilon = \omega_b \pm |J|, \tag{10}$$

and in the backward direction,

$$\epsilon = \omega_b \mp \Omega \pm \sqrt{\Omega^2 + |J|^2}. \tag{11}$$

Such direction dependency of the quasi-energy levels as a function of J is shown in Fig. 2(b). Due to phase-matched coupling, the Rabi splitting is much more prominent for the forward modes than the backward modes. Thus, at a given modulation strength J_0 as schematically shown in Fig. 2(b), an input with frequency at ω^* can be resonant with the Floquet modes and thus strongly couples to the ring in the backward direction, but the same input would be off resonant to the Floquet modes and thus decouples from the ring in the forward direction. The difference between forward and backward directions results in a direction dependent dissipation for the incident wave, which will be discussed in the next section.

C. Coupled Mode Analysis of a Direction-dependent Dissipation

We now describe the direction-dependent dissipation using the temporal coupled mode theory [31], [32]. As an illustration, we schematically show the input and output amplitudes as well as the modal amplitudes in Fig. 2(c). The input wave that is sent through the straight waveguide has a form $s_{\text{in}}^+ e^{i\omega_0 t}$ in the forward direction, and $s_{\text{in}}^- e^{i\omega_0 t}$ in the backward direction, where ω_0 is the input frequency, and $s_{\text{in}}^{\pm}$ is the incident wave amplitude. Meanwhile, we define $\alpha^{\pm}(t)$ and $\beta^{\pm}(t)$ as the amplitudes of modes $|a^{\pm}\rangle$ and $|b^{\pm}\rangle$, respectively. Under a modulation as represented in (3), the dynamics of $\alpha^{\pm}(t)$ and $\beta^{\pm}(t)$ can be written as

$$\begin{aligned} \frac{d}{dt} \begin{pmatrix} \alpha^{\pm} \\ \beta^{\pm} \end{pmatrix} &= \begin{pmatrix} i\omega_a - \gamma_a & 0 \\ 0 & i\omega_b - \gamma_b \end{pmatrix} \begin{pmatrix} \alpha^{\pm} \\ \beta^{\pm} \end{pmatrix} \\ &\quad + iV\cos(\Omega t + \phi) \begin{pmatrix} \alpha^{\pm} \\ \beta^{\pm} \end{pmatrix} + \begin{pmatrix} k_a \\ k_b \end{pmatrix} s_{\text{in}}^{\pm} e^{i\omega_0 t}, \end{aligned} \tag{12}$$

where γ_a and γ_b are the loss rate of modes $|a^{\pm}\rangle$ and $|b^{\pm}\rangle$, respectively, and k_a and k_b are the coupling rate from the external input into modes $|a^{\pm}\rangle$ and $|b^{\pm}\rangle$, respectively. The modulation at frequency Ω can excite many sideband frequency components at frequencies $\omega_n \equiv \omega_0 + n\Omega$, where n is the order of the sideband. Therefore, in steady state, we expand $\alpha^{\pm}(t)$ and $\beta^{\pm}(t)$ in terms of Fourier components:

$$\alpha^{\pm}(t) = e^{i\omega_0 t} \sum_n \alpha_n^{\pm} e^{in\Omega t}, \tag{13}$$

$$\beta^{\pm}(t) = e^{i\omega_0 t} \sum_n \beta_n^{\pm} e^{in\Omega t}, \tag{14}$$

where $\alpha_n^{\pm}$ and $\beta_n^{\pm}$ are time-independent the modal amplitude for $\alpha^{\pm}(t)$ and $\beta^{\pm}(t)$ at sideband frequency ω_n. We substitute (13) and (14) into (12), and after taking into account the modulation-induced coupling in (6), we can write the modal amplitudes in the forward direction as

$$\begin{pmatrix} i\Delta\omega_b + \gamma_a & -i\,J \\ -i\,J^* & i\Delta\omega_b + \gamma_b \end{pmatrix} \begin{pmatrix} \alpha_{-1}^+ \\ \beta_0^+ \end{pmatrix} = \begin{pmatrix} 0 \\ \kappa_b \end{pmatrix} s_{\text{in}}^+, \tag{15}$$

$$\begin{pmatrix} i\Delta\omega_a + \gamma_a & -i\,J \\ -i\,J^* & i\Delta\omega_a + \gamma_b \end{pmatrix} \begin{pmatrix} \alpha_0^+ \\ \beta_1^+ \end{pmatrix} = \begin{pmatrix} \kappa_a \\ 0 \end{pmatrix} s_{\text{in}}^+, \tag{16}$$

where $\Delta\omega_{a,b} \equiv \omega_0 - \omega_{a,b}$, and the modal amplitudes in the backward directions are

$$\begin{pmatrix} i\Delta\omega_a + \gamma_a & -i\,J^* \\ -i\,J & i\,(\Delta\omega_a - 2\Omega) + \gamma_b \end{pmatrix} \begin{pmatrix} \alpha_0^- \\ \beta_{-1}^- \end{pmatrix} = \begin{pmatrix} \kappa_a \\ 0 \end{pmatrix} s_{\text{in}}^-, \tag{17}$$

$$\begin{pmatrix} i\,(\Delta\omega_b + 2\Omega) + \gamma_a & -i\,J^* \\ -i\,J & i\Delta\omega_b + \gamma_b \end{pmatrix} \begin{pmatrix} \alpha_1^- \\ \beta_0^- \end{pmatrix} = \begin{pmatrix} 0 \\ \kappa_b \end{pmatrix} s_{\text{in}}^-. \tag{18}$$

From above, the steady-state forward modal amplitudes are calculated as

$$\alpha_{-1}^{+} = \frac{iJk_b}{D_1} s_{\text{in}}^{+}, \tag{19a}$$

$$\beta_{0}^{+} = \frac{(i\Delta\omega_b + \gamma_a)\, k_b}{D_1} s_{\text{in}}^{+}, \tag{19b}$$

$$\alpha_{0}^{+} = \frac{(i\Delta\omega_a + \gamma_b)\, k_a}{D_2} s_{\text{in}}^{+}, \tag{19c}$$

$$\beta_{1}^{+} = \frac{iJ^{*}k_a}{D_2} s_{\text{in}}^{+}, \tag{19d}$$

$$D_1 = (i\Delta\omega_b + \gamma_a)(i\Delta\omega_b + \gamma_b) + |J|^2, \tag{19e}$$

$$D_2 = (i\Delta\omega_a + \gamma_a)(i\Delta\omega_a + \gamma_b) + |J|^2, \tag{19f}$$

and the backward modal amplitudes are calculated as

$$\beta_{-1}^{-} = \frac{i\ J\ k_a}{D_3} s_{\text{in}}^{-}, \tag{20a}$$

$$\alpha_{0}^{-} = \frac{(i\,(\Delta\omega_a - 2\Omega) + \gamma_b)\, k_a}{D_3} s_{\text{in}}^{-}, \tag{20b}$$

$$\beta_{0}^{-} = \frac{(i\,(\Delta\omega_b + 2\Omega) + \gamma_a)\, k_b}{D_4} s_{\text{in}}^{-}, \tag{20c}$$

$$\alpha_{1}^{-} = \frac{i\ J^{*}\ k_b}{D_4} s_{\text{in}}^{-}, \tag{20d}$$

$$D_3 = (i\Delta\omega_a + \gamma_a)(i\,(\Delta\omega_a - 2\Omega) + \gamma_b) + |J|^2, \tag{20e}$$

$$D_4 = (i\Delta\omega_b + \gamma_b)(i\,(\Delta\omega_b + 2\Omega) + \gamma_a) + |J|^2. \tag{20f}$$

Given the steady-state modal amplitudes, the output (transmitted) amplitudes in the forward and backward directions, $s_{\text{out}}^{\pm}(t)$, can be expressed as [31]

$$s_{\text{out}}^{\pm}(t) = -s_{\text{in}}^{\pm} e^{i\omega_0 t} + \begin{pmatrix} k_a & k_b \end{pmatrix} \begin{pmatrix} \alpha^{\pm}(t) \\ \beta^{\pm}(t) \end{pmatrix}, \tag{21}$$

Therefore, from (19) and (20), $s_{\text{out}}^{\pm}(t)$ in (21) contains only frequency components at $\omega_0 - \Omega$, ω_0, and $\omega_0 + \Omega$. For nonzero $|J|$, the solution for $\begin{pmatrix} \alpha^{+}(t) \\ \beta^{+}(t) \end{pmatrix}$ is different from $\begin{pmatrix} \alpha^{-}(t) \\ \beta^{-}(t) \end{pmatrix}$. Thus, the transmission and dissipation for an input at ω_0 in opposite directions are different.

As an example of the nonreciprocal dissipation, we can calculate the forward and backward transmission spectrum at a given modulation strength. We fix the modulation-induced coupling term to be $J_0 = 0.25\Omega$, and we vary the incident frequency ω_0 and observe its transmission in both the forward and backward directions. The transmission spectra at each output sideband frequency, $\omega_n \equiv \omega_0 + n\Omega$, are plotted in Fig. 2(d), from which we observe that the forward and backward waves couple to different Floquet resonances, as indicated by locations where the transmission at ω_0 experiences significant dissipation. The dotted black lines in Fig. 2(d) indicate the locations of the Floquet quasi-energies in (10) and (11), which accurately capture the Floquet resonances in the modulated structure after the nonreciprocal Rabi splitting. In particular, we notice that at frequency ω^* that is slightly blue-shifted from ω_b and corresponds to the Floquet quasi-energy in the backward direction, there is almost no transmission in the backward direction at all frequencies, whereas in the forward direction at ω^*, there is significant transmission. Therefore, the coupled mode analysis shows that the modulated ring resonator in Fig. 1(a) can result in a nonreciprocal Rabi splitting, which can be used to achieve direction-dependent transmission and dissipation.

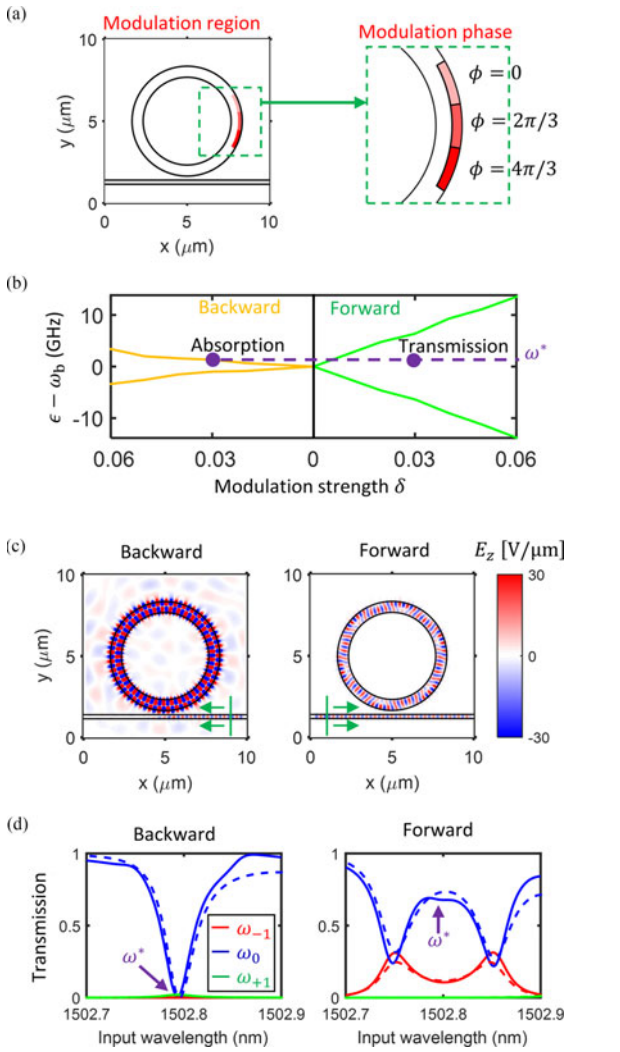

Fig. 3. (a) Schematics of the modulation region of the ring resonator. (b) Floquet quasi-energies of the modulated ring as simulated using MF-FDFD, which agree very well with Fig. 2(b). At an input frequency ω^* and a modulation strength $\delta = 0.03$, we expect to see nonreciprocal optical absorption. (c) Field profiles for both backward and forward modes at modulation strength of $\delta = 0.03$ for an input wave at frequency ω^*. The modulation results in full absorption in the backward direction, but high transmission in the forward direction. (d) Transmission spectrum of the ring resonator as simulated using MF-FDFD (solid lines) and compared with coupled mode theory (dotted lines) in both forward and backward directions.

III. Numerical Demonstration

Having discussed the theoretical analyses for nonreciprocal absorption using direction-dependent Rabi splitting, we now demonstrate this phenomenon through a rigorous full-wave simulation of the ring resonator in Fig. 1(a) using the multi-frequency finite-difference frequency-domain (MF-FDFD) algorithm [33]. The simulation setup is the same as that for the passive structure in Section II-A. We implement the permittivity modulation on one-sixth of the ring as described by (1), with the modulation phase profile, $\varphi(\mathbf{r})$, as shown in Fig. 3(a). The modulation occurs only at the outer half of the ring waveguide

in order to significantly couple modes $|a^{\pm}\rangle$ and $|b^{\pm}\rangle$, which are approximately even and odd with respect to the center of the waveguide. The modulation phase is separated into three blocks, where each block's phase differs by $2\pi/3$. This provides $\varphi(\boldsymbol{r})$ with an azimuthal momentum $M = m_b - m_a = -6$, which induces a phase-matched coupling between modes $|a^{+}\rangle$ and $|b^{+}\rangle$ that is phase-mismatched between $|a^{-}\rangle$ and $|b^{-}\rangle$.

To observe the nonreciprocal Rabi splitting, we send in forward and backward propagating waves at various frequencies near ω_b from the straight waveguide into the ring. From the coupled mode theory analysis above, the input frequencies where we observe significant dissipation should indicate the locations of Floquet quasi-energies. Thus, by performing such simulations where we vary the modulation strength δ from 0 to 0.06, we can plot the Floquet quasi-energies as a function of modulation strength for both forward and backward propagating directions, as shown in Fig. 3(b). This plot clearly exhibits the effect of the direction-dependent Rabi splitting as predicted above. It further shows excellent agreement with the theoretical descriptions of (10) and (11) and the plot in Fig. 2(b).

To use such nonreciprocal Rabi splitting for direction-dependent optical dissipation, we can examine the transmission spectrum with permittivity modulation strength of, for example, $\delta = 0.03$, which roughly corresponds to the coupling strength of $J = 0.25\Omega$ in (6). Such a modulation strength can be obtained with realistic silicon electro-optic modulation schemes [34], [35]. From Fig. 3(b), we expect an input wave at frequency ω^*, which is upshifted by 1.3 GHz from ω_b, to be significantly transmitting in the forward direction because it is far away from the Floquet resonance, whereas a backward wave at the same frequency would be fully dissipated by the ring because ω^* is resonant with the Floquet resonance of the ring. In Fig. 3(c), we plot the field patterns of the modulated structure as an input wave at ω^* is sent in from both directions. In the backwards propagation, the input wave strongly couples to the ring and has very low transmission through the ring. On the other hand, a forward wave sent in at ω^* does not strongly excite the modes of the ring resonator and has significantly higher transmission through the ring.

In Fig. 3(d), we vary the input frequency around ω^* and plot the spectrum of each transmitted frequency component in both forward and backward directions. The transmission spectra show excellent agreement with coupled mode theory predictions (dotted lines). Using this figure, we find that the isolation ratio, defined as the ratio of the power at the input frequency between the forward and backward transmission, has a 10 dB bandwidth of 1.3 GHz, which is mainly limited by the intrinsic linewidth of the ring resonator mode at frequency ω_b. From the simulation results above, we demonstrate that the dynamic modulation can directly produce the direction-dependent Rabi splitting effect and enable nonreciprocal optical dissipation.

IV. Conclusion

In summary, we have designed and demonstrated nonreciprocal optical dissipation based on direction-dependent Rabi splitting. In all the analyses above, as a proof of principles we performed two-dimensional numerical computations for a waveguide-ring system in the transverse-magnetic polarization. However, the theory for the direction-dependent Rabi splitting is general and can be applicable to the transverse-electric polarization as well as to three dimensional resonator structures. As long as the resonator supports two lossy traveling-wave modes, a spatiotemporal modulation with the appropriate momentum can break time-reversal symmetry and induce nonreciprocal absorption that suppresses backward wave propagation while transmitting forward waves. This type of nonreciprocal optical dissipation should prove to be useful in the design of optical isolators for optical communication systems or on-chip optical signal processing.

We end our paper by discussing the connection and contrast between our work and two recent related works by Kim, *et al*. [20] and Sohn, *et al*. [21]. In [20], a nonreciprocal dissipation is achieved through the use of stimulated Brillouin scattering. The structure consists of a whispering gallery resonator that is critically coupled to an external waveguide and is excited with a forward control laser. Through Brillouin scattering with the forward laser, a second wave sent from the forward direction generates a phase-matched acoustic wave inside the resonator that results in a strong acousto-optics modulation, which allows the wave to bypass the resonator through Brillouin scattering induced transparency. On the other hand, the same second wave sent from the backward direction does not resonantly excite an acoustic mode in the resonator. The wave hence does not experience acousto-optic modulation inside the resonator, and it is thereby absorbed and dissipated. In contrast, our present work provides a nonreciprocal dissipation in the presence of a dynamic modulation for both forward and backward waves.

In [21], a nonreciprocal frequency-shifting isolator was experimentally demonstrated using photonic transition in a multimode resonator enabled by an acousto-optic modulation. Refractive index modulation provided by an acoustic pump enables mode coupling in only one direction, and the system was studied using a coupled mode theory formalism similar to the one presented here. In the present work, however, the Floquet analysis highlights nuanced features that were unaccounted for in previous coupled mode theory treatment. For example, it was previously thought that a large phase-mismatched photonic transition in a resonator would not significantly alter its properties. However, our Floquet analysis reveals that such phase-mismatched photonic transition can noticeably shift the eigen-frequency spectrum of the system. Since this shift is comparable to the isolation ratio linewidth, it affects the design and performance of such isolators.

References

[1] H. A. Haus, *Waves and Fields in Optoelectronics*. Englewood Cliffs, NJ: Prentice Hall, 1983.
[2] D. Jalas *et al.*, "What is—and what is not—an optical isolator," *Nat. Photon.*, vol. 7, no. 8, pp. 579–582, Aug. 2013.
[3] Y. Shi, Z. Yu, and S. Fan, "Limitations of nonlinear optical isolators due to dynamic reciprocity," *Nat. Photon.*, vol. 9, no. 6, pp. 388–392, Jun. 2015.
[4] H. Iwamura, S. Hayashi, and H. Iwasaki, "A compact optical isolator using a $Y_3Fe_5O_{12}$ crystal for near infra-red radiation," *Opt. Quantum Electron.*, vol. 10, no. 5, pp. 393–398, Sep. 1978.
[5] K. Shiraishi, S. Sugaya, and S. Kawakami, "Fiber Faraday rotator," *Appl. Opt.*, vol. 23, no. 7, pp. 1103–1106, Apr. 1984.

[6] Y. Shoji and T. Mizumoto, "Magneto-optical non-reciprocal devices in silicon photonics," *Sci. Technol. Adv. Mater.*, vol. 15, no. 1, p. 014602, 2014.
[7] M.-C. Tien, T. Mizumoto, P. Pintus, H. Kromer, and J. E. Bowers, "Silicon ring isolators with bonded nonreciprocal magneto-optic garnets," *Opt. Express*, vol. 19, no. 12, pp. 11740–11745, Jun. 2011.
[8] L. Bi *et al.*, "On-chip optical isolation in monolithically integrated non-reciprocal optical resonators," *Nat. Photon.*, vol. 5, no. 12, pp. 758–762, Dec. 2011.
[9] S. Ghosh *et al.*, "Ce:YIG/Silicon-on-Insulator waveguide optical isolator realized by adhesive bonding," *Opt. Express*, vol. 20, no. 2, pp. 1839–1848, Jan. 2012.
[10] Z. Yu and S. Fan, "Complete optical isolation created by indirect interband photonic transitions," *Nat. Photon.*, vol. 3, no. 2, pp. 91–94, Feb. 2009.
[11] K. Fang, Z. Yu, and S. Fan, "Photonic Aharonov–Bohm effect based on dynamic modulation," *Phys. Rev. Lett.*, vol. 108, no. 15, p. 153901, Apr. 2012.
[12] A. Shaltout, A. Kildishev, and V. Shalaev, "Time-varying metasurfaces and Lorentz non-reciprocity," *Opt. Mater. Express*, vol. 5, no. 11, pp. 2459–2467, Nov. 2015.
[13] D. L. Sounas and A. Alù, "Angular-momentum-biased nanorings to realize magnetic-free integrated optical isolation," *ACS Photon.*, vol. 1, no. 3, pp. 198–204, Mar. 2014.
[14] N. A. Estep, D. L. Sounas, J. Soric, and A. Alù, "Magnetic-free non-reciprocity and isolation based on parametrically modulated coupled-resonator loops," *Nat. Phys.*, vol. 10, no. 12, pp. 923–927, Dec. 2014.
[15] H. Lira, Z. Yu, S. Fan, and M. Lipson, "Electrically driven nonreciprocity induced by interband photonic transition on a silicon chip," *Phys. Rev. Lett.*, vol. 109, no. 3, p. 033901, Jul. 2012.
[16] L. D. Tzuang, K. Fang, P. Nussenzveig, S. Fan, and M. Lipson, "Non-reciprocal phase shift induced by an effective magnetic flux for light," *Nat. Photon.*, vol. 8, no. 9, pp. 701–705, Sep. 2014.
[17] C. R. Doerr, L. Chen, and D. Vermeulen, "Silicon photonics broadband modulation-based isolator," *Opt. Express*, vol. 22, no. 4, pp. 4493–4498, Feb. 2014.
[18] E. Li, B. J. Eggleton, K. Fang, and S. Fan, "Photonic Aharonov–Bohm effect in photon–phonon interactions," *Nat. Commun.*, vol. 5, p. 3225, Jan. 2014.
[19] J. Kim, M. C. Kuzyk, K. Han, H. Wang, and G. Bahl, "Non-reciprocal Brillouin scattering induced transparency," *Nat. Phys.*, vol. 11, no. 3, p. 275, Mar. 2015.
[20] J. Kim, S. Kim, and G. Bahl, "Complete linear optical isolation at the microscale with ultralow loss," *Sci. Rep.*, vol. 7, May 2017.
[21] D. B. Sohn, S. Kim, and G. Bahl, "Time-reversal symmetry breaking with acoustic pumping of nanophotonic circuits," *Nat. Photon.*, vol. 12, no. 2, pp. 91–97, Feb. 2018.
[22] L. Kuhn, P. F. Heidrich, and E. G. Lean, "Optical guided wave mode conversion by an acoustic surface wave," *Appl. Phys. Lett.*, vol. 19, no. 10, pp. 428–430, Nov. 1971.
[23] I. K. Hwang, S. H. Yun, and B. Y. Kim, "All-fiber-optic nonreciprocal modulator," *Opt. Lett.*, vol. 22, no. 8, pp. 507–509, Apr. 1997.
[24] Y. Shi, S. Han, and S. Fan, "Optical circulation and isolation based on indirect photonic transitions of guided resonance modes," *ACS Photon.*, vol. 4, no. 7, pp. 1639–1645, Jul. 2017.
[25] W. Shin and S. Fan, "Choice of the perfectly matched layer boundary condition for frequency-domain Maxwell's equations solvers," *J. Comput. Phys.*, vol. 231, no. 8, pp. 3406–3431, Apr. 2012.
[26] G. Veronis, R. W. Dutton, and S. Fan, "Method for sensitivity analysis of photonic crystal devices," *Opt. Lett.*, vol. 29, no. 19, pp. 2288–2290, Oct. 2004.
[27] J.-P. Berenger, "A perfectly matched layer for the absorption of electromagnetic waves," *J. Comput. Phys.*, vol. 114, no. 2, pp. 185–200, Oct. 1994.
[28] J. N. Winn, S. Fan, J. D. Joannopoulos, and E. P. Ippen, "Interband transitions in photonic crystals," *Phys. Rev. B*, vol. 59, no. 3, pp. 1551–1554, Jan. 1999.
[29] J. O. Hirschfelder, R. E. Wyatt, and R. D. Coalson, Eds., *Advances in Chemical Physics, Volume 73: Lasers, Molecules, and Methods*, 1 ed., New York, NY, USA: Wiley, 1989.
[30] B. W. Shore, *Manipulating Quantum Structures Using Laser Pulses*, 1 edn., Cambridge, U.K.: Cambridge University Press, 2011.
[31] W. Suh, Z. Wang, and S. Fan, "Temporal coupled-mode theory and the presence of non-orthogonal modes in lossless multimode cavities," *IEEE J. Quantum Electron.*, vol. 40, no. 10, pp. 1511–1518, Oct. 2004.
[32] M. Minkov, Y. Shi, and S. Fan, "Exact solution to the steady-state dynamics of a periodically modulated resonator," *APL Photon.*, vol. 2, no. 7, p. 076101, Jun. 2017.
[33] Y. Shi, W. Shin, and S. Fan, "Multi-frequency finite-difference frequency-domain algorithm for active nanophotonic device simulations," *Optica*, vol. 3, no. 11, pp. 1256–1259, Nov. 2016.
[34] G. T. Reed *et al.*, "Recent breakthroughs in carrier depletion based silicon optical modulators," *Nanophoton.*, vol. 3, no. 4–5, pp. 229–245, 2013.
[35] R. Soref and B. Bennett, "Electrooptical effects in silicon," *IEEE J. Quantum Electron.*, vol. QE-23, no. 1, pp. 123–129, Jan. 1987.

Yu Shi received the B.S. degree in electrical engineering from The Ohio State University, Columbus, OH, USA, in 2013, and the M.S. degree in electrical engineering in 2015 from Stanford University, Stanford, CA, USA, where he is currently working toward the Ph.D. degree in electrical engineering.

He has authored or coauthored more than 10 refereed journal articles. His research interests include optical isolation, metamaterials and metasurfaces, thermal management with photonics, and computational electromagnetics.

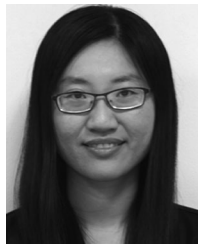

Qian Lin received the B.S. degree in physics from the Massachusetts Institute of Technology, Cambridge, MA, USA, in 2013, and the M.S. degree in electrical engineering in 2018 from Stanford University, Stanford, CA, USA, where she is currently working toward the Ph.D. degree in applied physics

Her research interests include theoretical and computational studies of optical nonreciprocity and topological effects in silicon photonics, metamaterials, and cold atoms.

Momchil Minkov received the B.S. degree in physics from Jacobs University Bremen, Bremen, Germany, in 2010, and the M.S. and Ph.D. degrees in physics from the Swiss National Polytechnic Institute in Lausanne, Lausanne, Switzerland, in 2012 and 2016, respectively. He is currently a Postdoctoral Research Associate with Stanford University, Stanford, CA, USA, under a fellowship from the Swiss National Science Foundation.

He has coauthored more than 15 peer-reviewed articles, and his research interests include photonic crystals and their applications, as well as time-modulated optical systems for integrated technologies and topological photonics.

Shanhui Fan (F'11) received the Ph.D. degree in theoretical condensed matter physics from the Massachusetts Institute of Technology (MIT), Cambridge, MA, USA, in 1997.

He is currently a Professor in electrical engineering, a Professor in applied physics (by courtesy), a Senior Fellow with the Precourt Institute of Energy, and the Director of the Edward L. Ginzton Laboratory, Stanford University, Stanford, CA, USA. He was a Research Scientist with the Research Laboratory of Electronics, MIT. He has authored or coauthored more than 400 refereed journal articles that were cited more than 35 000 times according to the Web of Sciences, has given more than 300 invited talks, and was granted 62 U.S. patents. His research interests include fundamental studies of solid state and photonic structures and devices, especially photonic crystals, plasmonics, and metamaterials, and their applications in information and energy technology.

Dr. Fan was the recipient of the National Science Foundation Career Award in 2002, the David and Lucile Packard Fellowship in Science and Engineering in 2003, the National Academy of Sciences Award for Initiative in Research in 2007, the Adolph Lomb Medal from the Optical Society of America in 2007, and the Vannevar Bush Faculty Fellowship in 2017. He has been listed as a highly cited Researcher in physics by Thomson Reuters since 2015. He is a Fellow of the American Physical Society, the Optical Society of America, and the SPIE.